Effective-medium theory for multilayer metamaterials: Role of near-field corrections

Tong Liu,[1,2] Shaojie Ma,[1,2] Bowen Yang,[3] Shiyi Xiao,[3,*] and Lei Zhou[1,2,†]

[1]*State Key Laboratory of Surface Physics, Key Laboratory of Micro and Nano Photonic Structures (Ministry of Education) and Physics Department, Fudan University, Shanghai 200433, China*

[2]*Academy for Engineering and Technology, Fudan University, Shanghai 200433, China*

[3]*Key Laboratory of Specialty Fiber Optics and Optical Access Networks, Joint International Research Laboratory of Specialty Fiber Optics and Advanced Communication, Shanghai Institute for Advanced Communication and Data Science, Shanghai University, Shanghai 200444, China*

(Received 14 February 2020; revised 28 October 2020; accepted 4 November 2020; published 23 November 2020)

Although many effective-medium theories have been proposed for studying metamaterials, most of them do not work well for multilayer metamaterials with *small* interlayer distances. Based on *rigorous* mode-expansion analyses on a model system consisting of multiple layers of subwavelength gratings, we identify that the failures of conventional effective-medium theories are caused by neglecting strong near-field couplings in homogenizing such systems. These understandings motive us to propose an alternative homogenization approach for strongly coupled multilayer metamaterials, in which predominant near-field corrections have been considered automatically. Our effective-medium theory can well describe multilayer metamaterials with arbitrary interlayer distances including particularly those systems for which conventional effective-medium theories fail. We finally extend our theory to multilayer metamaterials with *complicated* microstructures and validate the theory by full-wave simulations as well as microwave experiments. Our theory not only well complements the available effective-medium theory formalisms, but also provides a powerful tool to study the properties of strongly coupled metamaterials, which may find many applications in practice.

DOI: 10.1103/PhysRevB.102.174208

I. INTRODUCTION

Metamaterials are man-made composite materials constructed by subwavelength-sized electromagnetic microstructures, which can exhibit tailored effective permittivity ε and permeability μ dictated by the details of microstructures. Metamaterials have attracted much attention recently due to their strong abilities to manipulate electromagnetic waves [1–4], generating fascinating effects such as negative refraction [5], superlensing [6,7], perfect light absorption [8–10], and polarization controls [11–13], which are difficult to realize with natural materials. In this research field, effective-medium theory (EMT) plays a crucial role since it serves as a bridge to link theoretical predictions (based on effective parameters) with practical realizations (based on realistic systems). Therefore, a good effective-medium theory, which can accurately retrieve the effective parameters of metamaterials with arbitrary microstructures, is always highly desired. A series of effective-medium theories has been developed for metamaterials in recent years, including *S*-parameters retrieval [14,15], field averaging [16,17], coherent-potential approximation and its generalizations [18–21], and so on. These approaches have been widely used in the community with great successes.

However, we note that these effective-medium theories do not always work well for metamaterials. In practical applications, occasionally one needs to stack multiple layers of microstructure array to form a bulk metamaterial [22–25], since usually a single layer does *not* yield the desired wave-manipulation effects. In studying these multilayer metamaterials, a commonly adopted approach is to first retrieve the effective-medium parameters of a carefully chosen subsystem (say, a single metallic layer plus appropriate spacers), and then use the obtained effective parameters to describe the whole multilayer metamaterial system [see Fig. 1(a)]. However, while such an approach can indeed work well for those metamaterials with one or few layer(s), derivations between its predictions and full-wave simulations significantly increase for metamaterials with more layers [Fig. 1(b)], not to mention the complexities in selecting a correct branch from multiple solutions of effective-medium parameters. Moreover, the deviations between theory and simulations become more significant in those metamaterials with smaller interslab distances [Fig. 1(c)], which are a bit counterintuitive at first glance since the effective-medium theory is supposed to work better for systems with better subwavelength properties. Such issues are intrinsic to conventional effective-medium theories, and cannot be solved by simply taking a larger subsystem (consisting of more layers) to determine the effective parameters [26,27]. In fact, one may even need to homogenize the whole system in order to get reasonable effective parameters if the multilayer metamaterials exhibit very small interlayer distances. Given the many potential applications of multilayer metamaterials, it is highly desired to establish an effective-medium theory to analyze such systems in a simple and reliable way.

*Corresponding author: phxiao@shu.edu.cn
†Corresponding author: phzhou@fudan.edu.cn

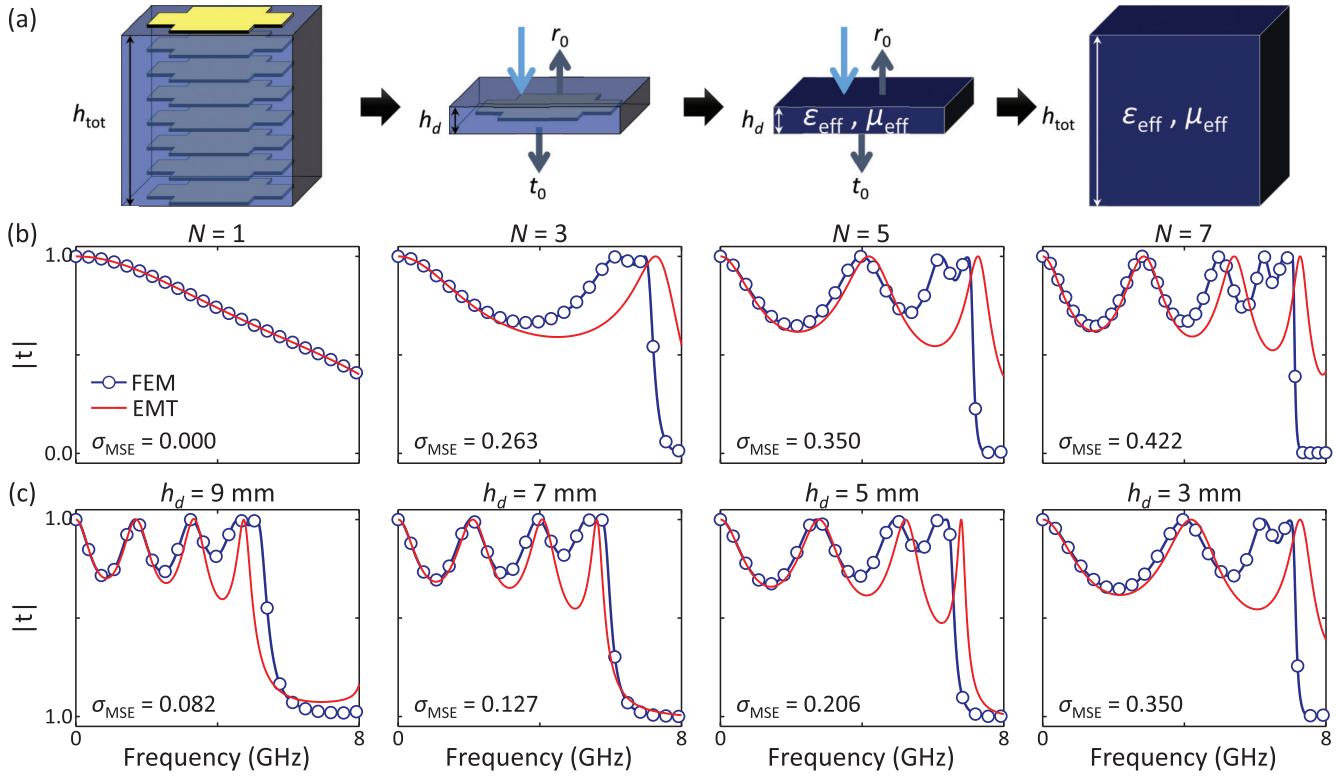

FIG. 1. (a) Schematics of the conventional effective-medium theory to determine the effective parameters of a multilayer metamaterial. Transmission spectra obtained by finite-element-method simulations (open circles) and the conventional effective-medium theory (red solid lines) for a series of N-layer metamaterials with (b) N changing from 1 to 7 with $h_d = 3$ mm fixed and for a series of N-layer metamaterials with (c) h_d changing from 9 to 3 mm with $N = 5$ fixed. A metallic layer contains a periodic array (with lattice constant 15 mm along two directions) of metallic crosses, each formed by two 0.018-mm-thick bars with width 5 mm and length 10 mm.

In this paper, we establish an alternative effective-medium theory formalism to study multilayer metamaterials with arbitrary interlayer distances. We first briefly describe in Sec. II the bottleneck issues faced by conventional effective-medium theories. Through analyzing a model system based on a *rigorous* mode-expansion method (MEM) in Sec. III, we identify that the failure of conventional effective-medium theories in studying multilayer metamaterials is caused by neglecting near-field couplings between metallic layers. In Sec. IV, inspired by the analytical results obtained with the mode-expansion method, we propose an alternative approach to retrieve the effective parameters of such multilayer metamaterials. Detailed comparisons with numerical simulations reveal that the effective-medium theory works well in a much wider parameter region than conventional effective-medium theories, since the predominant near-field couplings have been taken into account. After extending our theory to general situations with microstructures exhibiting complex shapes (Sec. V), supported by both full-wave simulations and microwave experiments, we conclude our paper in Sec. VI.

II. ISSUES IN CONVENTIONAL EFFECTIVE-MEDIUM THEORY

We start from quantitatively studying a concrete example to illustrate the issues in conventional effective-medium theories. Without losing generality, we assume that the metamaterial under study consists of N layers of a metallic "cross" array separated by dielectric spacers with permittivity $\varepsilon_d = 4.3$ and interlayer distance h_d. Such metamaterials are widely used to realize high-index materials in different frequency regimes [17,28–30].

To obtain the effective-medium properties of the metamaterials under study, we follow the typical strategy to first choose a single metallic layer sandwiched by two spacer layers with thickness $h_d/2$ [see Fig. 1(a)], and then retrieve its effective-medium parameters by the S-parameter retrieval method. The effective parameters thus obtained are supposed to describe the metamaterials with arbitrary thicknesses. However, as we use such parameters to compute the transmission spectra of N-layer metamaterials with N changing from 1 to 7, we find that significant deviations exist between the effective-medium-theory results (solid lines) and those calculated by finite-element-method (FEM) simulations on realistic structures (open circles) as long as $N > 1$ [see Fig. 1(b)]. To quantitatively measure such discrepancies, we define the mean squared error (MSE) between two calculated spectra as $\sigma_{\rm MSE} = \int_{f_{\rm min}}^{f_{\rm max}} [|r_{\rm EMT} - r_{\rm FEM}|^2 + |t_{\rm EMT} - t_{\rm FEM}|^2] df/(f_{\rm max} - f_{\rm min})$, where $\{r_{\rm EMT}, t_{\rm EMT}\}$ and $\{r_{\rm FEM}, t_{\rm FEM}\}$ denote the reflection and transmission coefficients calculated by the effective-medium theory and numerical simulations, respectively, and $[f_{\rm min}, f_{\rm max}]$ is the frequency region of interest. Obviously,

σ_{MSE} increases significantly as N becomes larger [see Fig. 1(b)], implying that the effective parameters thus obtained do *not* work well for bulk metamaterials.

Moreover, we find that such discrepancies are larger in metamaterials with thinner spacers. As illustrated in Fig. 1(c), repeating the same analyses as in Fig. 1(b) on metamaterials with the same number of layers ($N = 5$) but with different interlayer distances, we find that σ_{MSE} increases significantly for systems with smaller h_d. Such effect is physically counterintuitive at first glance since an effective-medium theory is usually supposed to work better for systems with better subwavelength properties.

We emphasize that such an issue is intrinsic to all conventional effective-medium theories. In principle, one can certainly retrieve the effective parameters based on *larger* subsystems to better fit finite-element-method calculations, but the parameters thus obtained are at the cost of more time-consuming calculations, and exhibit less clear physical meanings. In what follows, still using *very thin* subsystems, we propose an alternative yet physically transparent approach to derive the effective parameters of multilayer metamaterials, which can better describe the metamaterials with larger thicknesses.

III. RIGOROUS ANALYSES ON A MODEL SYSTEM

We now choose a model metamaterial, which can be analytically solved by the mode-expansion method, to reveal the underlying physics. The analytical results obtained with such a model system can not only help identify the inherent reasons accounting for the failure of conventional effective-medium theories, but more importantly, also point out a route to solve the problem. As schematically shown in Fig. 2(a), the metamaterial consists of three layers of metallic gratings (with thickness h_m) separated by two dielectric spacers (with thickness h_d and permittivity ε_d). The periodicity of the grating is P, while the gap between two adjacent metallic stripes is a. The structure is invariant along the y direction. In the wavelength regime where $P \ll \lambda$ and $h_d + h_m \ll \lambda$, the whole system can be homogenized as an effective medium. In this paper, we only consider the low-frequency domain (e.g., GHz regime) where metals can be treated as perfect electric conductors.

We now study the scattering properties of the system under normal illumination of a transverse-magnetic (TM) polarized plane wave with $\vec{H} \parallel \hat{y}$. Here, the $z = 0$ plane is defined at the top surface of region III. Following the standard mode-expansion method [31–34], we expand electromagnetic waves in different regions to linear combinations of eigenmodes in those regions [see Fig. 2(a)]. For example, while electromagnetic eigenmodes in regions I, III, V, and VII are plane waves with different diffraction orders, they must be appropriate waveguide modes inside the slits in the regions labeled as II, IV, and VI. By matching the boundary conditions at the interfaces between two adjacent regions, we get a set of coupled linear equations to determine all expansion coefficients representing the strengths of these modes. Solving the coupled linear equations, we thus obtain the scattering properties of the whole system, including the coefficients of reflected and transmitted modes in different diffraction channels repre-

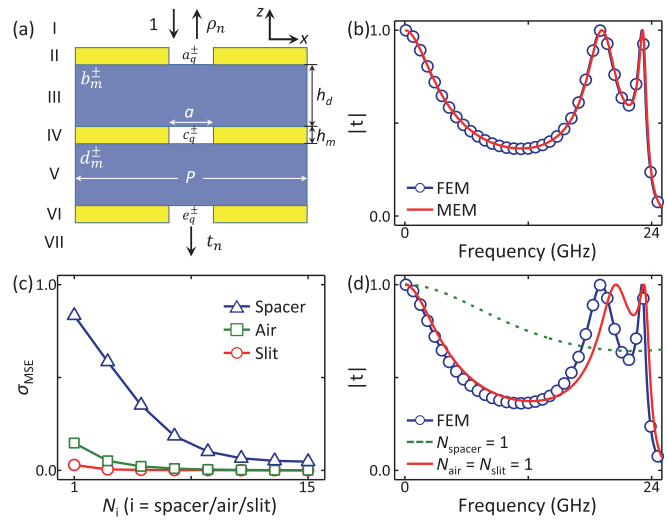

FIG. 2. (a) Schematics of the three-layer model metamaterial under study with geometric parameters given by $a = 0.2$ mm, $P = 3$ mm, $h_m = 0.018$ mm, $h_d = 0.4$ mm. The permittivity of the spacer is $\varepsilon_d = 4.3$. (b) Spectra of transmission amplitude calculated by finite-element-method simulations (blue open circles) and rigorous mode-expansion method (red solid line). (c) Calculated σ_{MSE} vs N_{spacer} (blue triangles), N_{air} (green squares), and N_{slit} (red circles), respectively. (d) Spectra of transmission amplitude calculated by finite-element-method simulations (blue open circles) and mode-expansion method with $N_{\mathrm{spacer}} = 1$ and $N_{\mathrm{air}} = N_{\mathrm{slit}} = 201$ (green line) and $N_{\mathrm{air}} = N_{\mathrm{slit}} = 1$ and $N_{\mathrm{spacer}} = 201$ (red line).

sented by ρ_n and t_n respectively (see Appendix A for detailed derivations). Although in principle we should take an infinite number of modes in different regions into our calculations, practically we only need to keep a finite number of modes in each region to ensure the computational convergence. We perform finite-element-method simulations to justify the developed mode-expansion method. Figure 2(b) compares the transmission spectra of such a metamaterial calculated by finite-element method and mode-expansion method, which agree with each other very well.

With such a powerful tool at hand, we now use it to reveal the physics underlying the failures of conventional effective-medium theories. As shown in Fig. 1(a), in the standard approach to determine the effective parameters, we first study the transmission/reflection properties of a single layer (appropriately cut from the multilayer system) and then map the system to a homogeneous slab with the same thickness [18,21]. Since no diffractions exist as a homogeneous slab is shined by a normally incident light, naturally one may expect that such mapping would be more reasonable as we "cut" the realistic sample at a position where all high-order diffractions are as weak as possible. Therefore, it is highly desired to explore the roles played by high-order modes in different regions in such a system.

To gain such information, we compute the σ_{MSE} of our system with different numbers of modes retained in three regions (denoted as N_{spacer}, N_{slit}, and N_{air}, respectively), and then depict in Fig. 2(c) how the calculated σ_{MSE} vary against these cutoff mode numbers. In all three cases, we find that increasing the cutoff numbers pushes the computed results

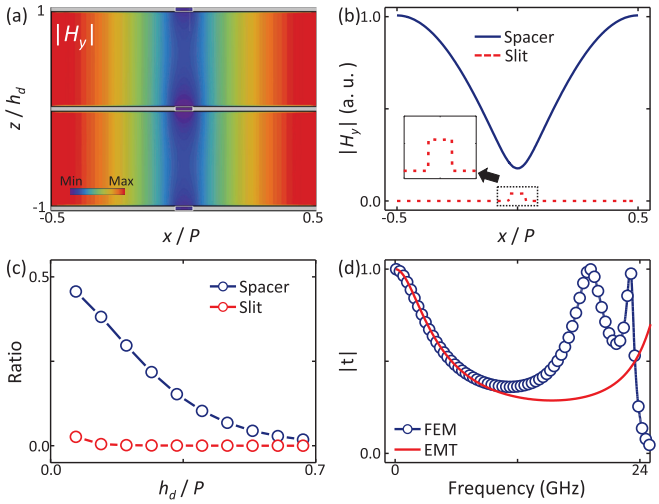

FIG. 3. (a) $|H_y|$ field distribution on an arbitrary $x-z$ plane inside the metamaterial, calculated by finite-element-method simulations at 23.02 GHz. (b) Computed $|H_y|$ field distributions along the central line in the spacer region (blue solid line) and along the central line across the metallic layer (red dashed line). (c) The ratios between energy flows carried by all high-order modes and that carried by the fundamental mode in the spacer (blue line) and the slit region (red line), calculated by the mode-expansion method for different values of h_d. (d) Spectra of transmission amplitude calculated by finite-element-method simulations (blue open circles) and the conventional effective-medium theory (red solid line).

to the numerically calculated one. However, the speeds to reach convergence with respect to increasing them are quite different. Specifically, the convergence against increasing N_{spacer} is ten times slower than increasing N_{slit} and N_{air} [see Fig. 2(c)], indicating that the high-order modes in the spacer regions play much more important roles than those in the other two regions. Indeed, the transmission spectrum calculated by the mode-expansion method assuming $N_{\text{slit}} = N_{\text{air}} = 1$ has already captured the key features of the finite-element-method-calculated spectrum [red line in Fig. 2(d)], while the same thing is not true as we set $N_{\text{spacer}} = 1$ [green line in Fig. 2(d)].

Such distinct convergence behaviors against different cutoff numbers can be understood as follows. Since our system is in subwavelength regime ($P \ll \lambda$), all high-order modes in two semi-infinite air regions below/above the sample (i.e., regions I and VII) must be evanescent waves and thus their contributions to the zero-order transmission/reflection coefficients are less important. Meanwhile, as we consider the thin-slit limit ($a \ll P$), all high-order waveguide modes in the slit regions have a very small overlap with plane waves in air or spacers, and thus their contributions to the final results are also not important. Such an argument is well supported by the finite-element-method-calculated field distribution inside a slit [Figs. 3(a) and 3(b)], which shows a very uniform distribution along the x direction, already implying that the total wave function mainly contains the fundamental transverse-electromagnetic (TEM) mode. However, high-order modes in the spacer regions, even being evanescent in nature, *cannot* be neglected as the spacer is thin, since they can have non-negligible contributions to the zero-order transmission/reflection coefficients through complicated multiple scatterings. Indeed, the field pattern inside the spacer region [Figs. 3(a) and 3(b)] exhibits a clear inhomogeneous feature, highlighting the important role played by the high-order evanescent modes. We note that the contribution of high-order modes becomes more significant as the spacer turns thinner, which is understandable since the coupling between evanescent modes belonging to adjacent layers becomes stronger in the thin-spacer limit [Fig. 3(c)]. Meanwhile, as the interlayer distance is larger than the decay length of the first high-order evanescent mode, the coupling between evanescent waves from two adjacent metallic layers is very weak and thus the final contributions of high order modes become less significant, as shown in Fig. 3(c).

The physical picture established above helps us understand why conventional effective-medium theories break down for multilayer metamaterials with small interlayer distances. In conventional approaches, typically the subsystem for homogenization is chosen to contain one or a few metallic layer(s) with appropriate spacer layers. However, in doing so one has to "cut" the original system at the positions (i.e., inside the spacer regions) where the near-field coupling effects are most significant [see Figs. 3(a)–3(c)]. As a result, the subsystem loses very important information (i.e., the near-field couplings) contained in the original system, which explains why the effective-medium theory thus established cannot well describe the original system [see Fig. 3(d)].

IV. DEVELOPMENT OF THE NEAR-FIELD-CORRECTED EFFECTIVE-MEDIUM THEORY

The physical understandings gained in the last section stimulate us to develop an *alternative* approach to homogenize the complex system, aiming to take the near-field couplings into consideration as much as possible. From Fig. 3(c), we find that the electromagnetic wave inside the slit region (region IV) mainly contains the fundamental waveguide mode while the strengths of high-order modes are very weak. This is because the thin-slit nature of the waveguide leads to

$$|S_{n0}|^2 \gg |S_{nq}|^2, \quad q \neq 0, \tag{1}$$

where S_{nq} denotes the coupling strength between the q th waveguide mode in the slit to the n th diffraction mode in the air or spacer region [34]. Equation (1) indicates that the strength of the excited fundamental mode must be much larger than that of high-order modes inside the slits. Therefore, for such metamaterial systems, if we choose the subsystem through "cutting" the realistic system at the middle planes inside a metallic layer [see Fig. 4(a)], then the strong near-field couplings in the spacers are fully taken into account. Meanwhile, such a cutting procedure does not drop too much information contributed by high-order modes in metallic layers, which are very weak anyway.

We now explicitly derive the effective-medium-theory formalism based on the homogenization process described above. As shown in Fig. 4(b), we first study the scattering properties of the chosen subsystem, shined by the zero-order mode allowed in the slit regions which are now assumed to be semi-infinite. Based on the mode-expansion method, we

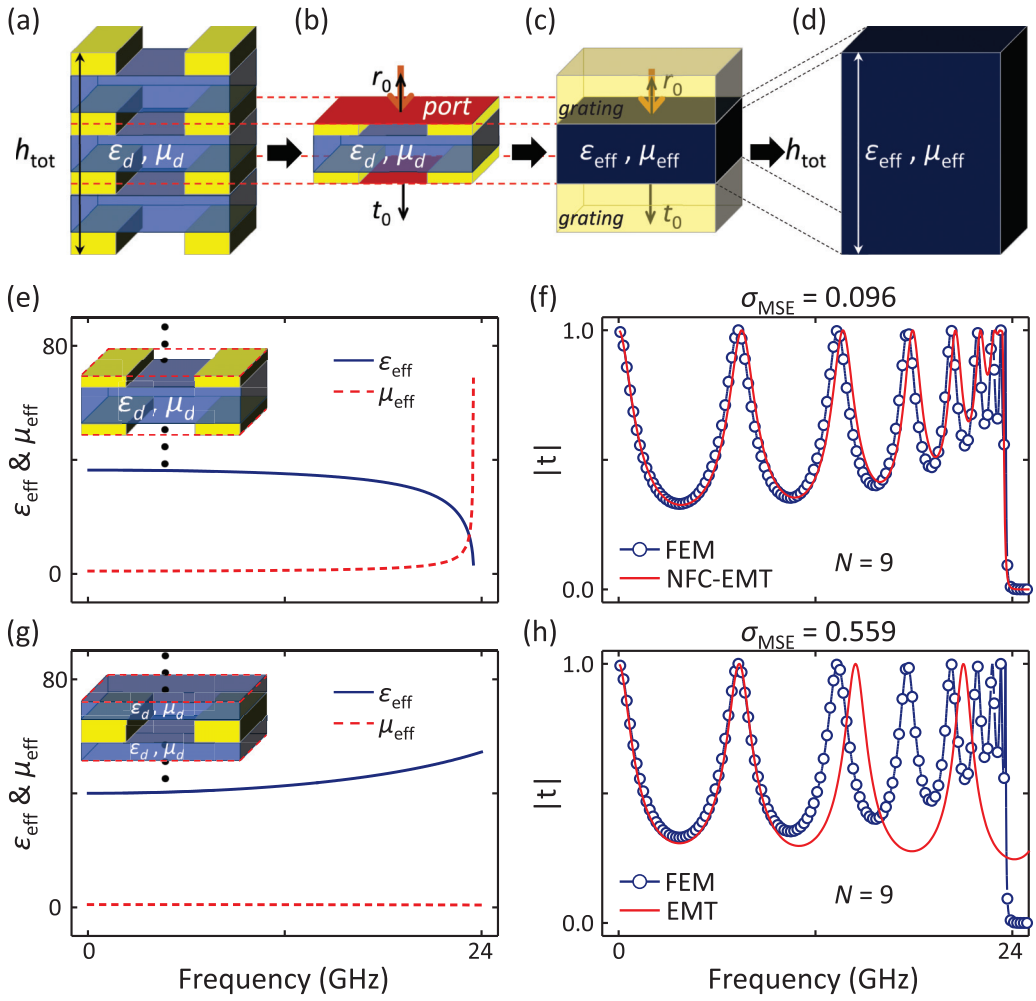

FIG. 4. (a)–(d) Schematics of retrieving the effective parameters of a multilayer metamaterial in the near-field-corrected effective-medium theory. (e),(g) Effective parameters retrieved by (e) the near-field-corrected effective-medium theory and (g) the conventional effective-medium theory. (f),(h) Transmission spectra computed by finite-element-method simulations (open circles), (f) the near-field-corrected effective-medium theory (red curves), and (h) the conventional effective-medium theory (red curves).

analytically obtain (see Appendix B for detailed derivations) that

$$\rho_0^{\text{single}} = -1 + \frac{1}{1+\alpha-\gamma} + \frac{1}{1+\alpha+\gamma}$$
$$t_0^{\text{single}} = \frac{2\gamma}{1+2\alpha+\alpha^2-\gamma^2}, \tag{2}$$

where $\alpha = i\sum_m |S_{m0}|^2 Y_m^{\text{III}}/Y_0^{\text{II}} \cot(k_{m,z}^{\text{III}} h_d)$ and $\gamma = i\sum_m |S_{m0}|^2 Y_m^{\text{III}}/Y_0^{\text{II}} \csc(k_{m,z}^{\text{III}} h_d)$, with $k_{m,z}^{\text{III}}$ representing the propagating wave vector of the m th diffraction mode in the spacer region and Y_m^{i} referring to the admittance of the m th eigenmode in region i. It is not surprising to see from Eq. (2) that all diffraction channels in the spacer region can contribute to the response of the whole system, since terms $\cot(k_{m,z}^{\text{III}} h_d)$ and $\csc(k_{m,z}^{\text{III}} h_d)$ just represent the multiple scatterings of the mth diffraction modes between two adjacent metallic layers.

We now map the subsystem to a homogenous slab with the same thickness. As shown in Fig. 4(c), in order to make such mapping reasonable, we study the electromagnetic response of a homogeneous slab (with effective parameters ε_{eff} and μ_{eff} to be determined), sandwiched by two semi-infinite materials representing the metallic gratings. Here, two semi-infinite background materials are modelled by a homogeneous effective medium with $\varepsilon_{\text{eff}}^{\text{slit}} = |S_{00}|^{-2}$ and $\mu_{\text{eff}}^{\text{slit}} = |S_{00}|^2$, obtained by the mode-expansion method under the single mode approximation [35]. A simple calculation yields the following expressions for the reflection/transmission coefficients of the model described in Fig. 4(c):

$$\rho_0^{\text{single}} = \frac{\left(Y_{\text{slit}}^2 - Y_{\text{eff}}^2\right)\sin(n_{\text{eff}} k_0 h_d)}{2iY_{\text{eff}}Y_{\text{slit}}\cos(n_{\text{eff}} k_0 h_d) + \left(Y_{\text{slit}}^2 + Y_{\text{eff}}^2\right)\sin(n_{\text{eff}} k_0 h_d)}$$
$$t_0^{\text{single}} = \frac{2iY_{\text{eff}}Y_{\text{slit}}}{2iY_{\text{eff}}Y_{\text{slit}}\cos(n_{\text{eff}} k_0 h_d) + \left(Y_{\text{slit}}^2 + Y_{\text{eff}}^2\right)\sin(n_{\text{eff}} k_0 h_d)}, \tag{3}$$

where $Y_{\text{slit}} = \sqrt{\varepsilon_{\text{eff}}^{\text{slit}}}/\sqrt{\mu_{\text{eff}}^{\text{slit}}} = |S_{00}|^{-2}$ is the effective admittance of the background medium, and Y_{eff} and n_{eff} are the effective admittance and refractive index of the metamaterial layer, respectively. Comparing Eq. (3) with Eq. (2), we

obtain

$$Y_{\text{eff}} = |S_{00}|^{-2}\sqrt{\alpha-\gamma}\sqrt{\alpha+\gamma}$$
$$n_{\text{eff}} = \frac{2}{k_0 h_d}\left[\tan^{-1}\left(i\frac{\sqrt{\alpha-\gamma}}{\sqrt{\alpha+\gamma}}\right)+g\pi\right], \quad (4)$$

with which we finally derive that

$$\varepsilon_{\text{eff}} = \frac{2}{k_0 h_d |S_{00}|^2}\sqrt{\alpha-\gamma}\sqrt{\alpha+\gamma}\left[\tan^{-1}\left(i\frac{\sqrt{\alpha-\gamma}}{\sqrt{\alpha+\gamma}}\right)+g\pi\right]$$
$$\mu_{\text{eff}} = \frac{2}{k_0 h_d}\frac{|S_{00}|^2}{\sqrt{\alpha-\gamma}\sqrt{\alpha+\gamma}}\left[\tan^{-1}\left(i\frac{\sqrt{\alpha-\gamma}}{\sqrt{\alpha+\gamma}}\right)+g\pi\right], \quad (5)$$

where $g \in Z$. Equation (5) gives the explicit forms of the effective parameters of the multilayer metamaterial under study, with the predominant part of near-field couplings successfully taken into account. We call such an effective-medium theory the near-field-corrected effective-medium theory (NFC-EMT), in order to differentiate it from the conventional effective-medium theory. Obviously, multiple solutions of effective-medium parameters exist due to the presence of g. In principle, we choose the correct branch based on the criterion that calculations on subsystems with different thicknesses should yield identical (at least nearly identical) solutions of effective-medium parameters. We find that the $g = 0$ branch for the one-layer subsystem is the correct branch, because the one-layer subsystem exhibits a deep-subwavelength thickness ($h_d \ll \lambda$) and thus the $g = 0$ branch naturally describes the fundamental mode propagating in such a subsystem. Moreover, the effective-medium parameters thus selected match very well with solutions found in subsystems containing more layers, simply because the present approach has already captured the predominant part of near-field couplings (see Appendix C for a detailed discussion).

We now check the validity of the near-field-corrected effective-medium theory by studying a realistic nine-layer metamaterial. The solid line in Fig. 4(f) represents the transmission spectrum of an effective-medium slab with ε_{eff} and μ_{eff} given in Fig. 4(e), derived from the near-field-corrected effective-medium theory. Compared to the numerically calculated transmission spectrum on the realistic structure [open circles in Fig. 4(f)], we find that results obtained with our theory have captured all essential features, reinforced by the small value of σ_{MSE} (0.096) between the two spectra. In sharp contrast, repeating all calculations based on the conventional effective-medium theory [Figs. 4(g) and 4(h)], we find that the difference between spectra calculated by effective-medium theory and the finite-element method is much larger ($\sigma_{\text{MSE}} = 0.559$). In fact, the effective parameters calculated by our theory [see Fig. 4(e)] exhibit very different, even opposite dispersion behaviors, as compared to those by the conventional effective-medium theory [Fig. 4(g)]. For example, while the μ_{eff} calculated by conventional effective-medium theory exhibits quite weak frequency dependence and is very close to 1, μ_{eff} derived by the near-field-corrected effective-medium theory, however, diverges at a particular frequency signifying the existence of a magnetic resonance. Such a magnetic resonance is formed by electric currents flowing in opposite directions on two metallic layers, which is automatically considered by our effective-medium theory.

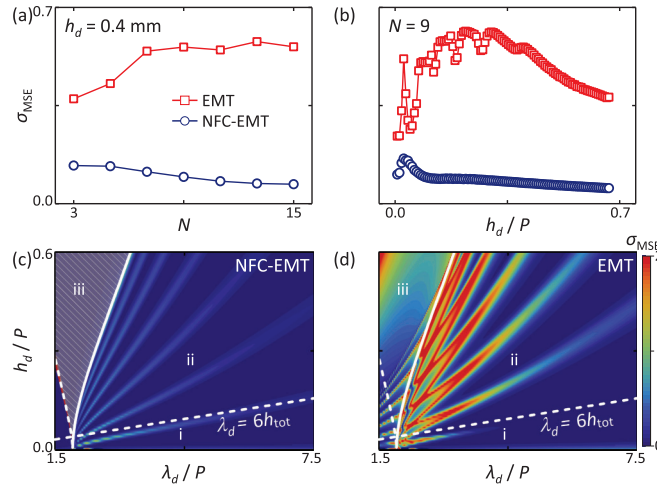

FIG. 5. (a),(b) σ_{MSE} calculated with the conventional effective-medium theory (red squares) and the near-field-corrected effective-medium theory (blue circles) for a series of N-layer metamaterials with (a) N changing from 3 to 15 with $h_d = 0.4$ mm fixed and another series of nine-layer metamaterials with (b) h_d changing from 0.02 to 2 mm. (c),(d) σ_{MSE} as functions of h_d and λ_d for the nine-layer metamaterials computed by (c) the near-field-corrected effective-medium theory and (d) the conventional effective-medium theory. Here, the white solid line denotes the wavelengths of the magnetic resonance for different h_d.

We continue to examine the performance of the near-field-corrected effective-medium theory by studying more metamaterials with different layers (N) and interlayer distance h_d. Figure 5(a) presents how σ_{MSE} varies against N, calculated by both our theory and the conventional theory. For all samples studied, near-field-corrected effective-medium theory always works much better than the conventional effective-medium theory, evidenced by much smaller values of σ_{MSE}. Interestingly, the larger N becomes, the better the near-field-corrected theory is as compared to the conventional effective-medium theory. We can understand such an intriguing result based on the following arguments. We note that our near-field-corrected theory does not consider the higher-order diffraction modes in two air regions above/below the sample, which is one possible source to generate discrepancies. However, such an interfacial effect has smaller relative contributions to the final results as N increases. Quite on the contrary, as N increases, the conventional effective-medium theory must get worse as it naturally neglects the interlayer couplings which can accumulate more errors as more layers are stacked. These different trends well explain why the advantages of the near-field-corrected theory are more dramatic in large-N samples [Fig. 5(a)]. Figure 5(b) illustrates how σ_{MSE} calculated by two methods vary against h_d for a series of nine-layer samples with different h_d. Again, we find that the near-field-corrected theory works better than the conventional effective-medium theory for all cases studied.

In order to gain deeper understandings, we now study the mean-square errors between results obtained by

effective-medium theory and finite-element method at *every* wavelength, defined by $\sigma_{\mathrm{MSE}}(\lambda_d) = |r_{\mathrm{EMT}} - r_{\mathrm{FEM}}|^2 + |t_{\mathrm{EMT}} - t_{\mathrm{FEM}}|^2$ with $\lambda_d = \lambda/\sqrt{\varepsilon_d}$ denoting the wavelength inside the spacer. Figures 5(c) and 5(d) depict, respectively, how $\sigma_{\mathrm{MSE}}(\lambda_d)$ varies against λ_d and h_d, calculated by two different versions of effective-medium theory for a series of nine-layer samples with different h_d. Comparisons between Figs. 5(c) and 5(d) clearly demonstrate that the near-field-corrected effective-medium theory works much better than the conventional effective-medium theory for all cases studied, represented by much smaller values of $\sigma_{\mathrm{MSE}}(\lambda_d)$ of near-field-corrected theory in the entire parameter space. In contrast, we find from Fig. 5(d) that $\sigma_{\mathrm{MSE}}(\lambda_d)$ can be quite large in certain spikelike regions where transmission resonances take place. To facilitate our further analyses, we add to the two figures an auxiliary line, defined by $\lambda_d = 6h_{\mathrm{tot}}$ with h_{tot} representing the total thickness of the sample. Such an auxiliary line together with the shadow region with properties discussed below divide the whole parameter region to three different subregions labeled by i, ii, and iii, respectively. We find that the near-field-corrected effective-medium theory is more advantageous in region ii, where the sample is thick enough to accumulate the errors caused by neglecting the near-field couplings. Meanwhile, in region i where h_{tot} is too thin, two effective-medium theories can both work well since the errors caused by neglecting near-field couplings do not accumulate to large-enough values. Finally, in region iii (the shadow region), the near-field-corrected effective-medium theory does not work well since the effective parameters obtained by Eq. (5) will contain imaginary parts. In fact, this region is tightly connected with the appearance of the magnetic resonance as discussed in Fig. 4(e), which makes the usual effective-medium description invalid for the metamaterial. Although one can still use the conventional effective-medium theory to derive the effective parameters of the metamaterial in this region, the obtained parameters cannot accurately describe the metamaterial, as demonstrated by the large $\sigma_{\mathrm{MSE}}(\lambda)$ values. In such regions with relatively strong scatterings, one has to use other methods (say, the quasimode approach [21]) to derive meaningful effective parameters for the metamaterials.

V. EXTENSIONS TO ARBITRARY STRUCTURES AND EXPERIMENTAL VALIDIFICATION

The theoretical formalism presented in last section, derived with a simple structure, can be extended to study general multilayer metamaterials. Take a multilayer metamaterial with unit microstructure being a metallic cross [see Fig. 6(a)] as an example; we follow the general homogenization strategy as described in the last section to derive its effective parameters. Comparing the present system to that studied in the last section, we find the following two differences: First, the fundamental eigenmode in the metallic region is no longer a transverse-electromagnetic waveguide mode, but rather a quasi- transverse-electromagnetic mode with field distribution given by $\vec{E}^{\mathrm{Floquet}}_{q=0}$, which can only be obtained by numerical simulations. Second, now an eigenmode in the spacer region should be labeled by three indices: $\{m_x, m_y\}$ describing the diffraction channel with parallel wave vector $\vec{k}_{||} = m_x G_x \hat{x} + m_y G_y \hat{y}$ where G_x and G_y are the reciprocal vectors along two directions, and σ denoting the polarization.

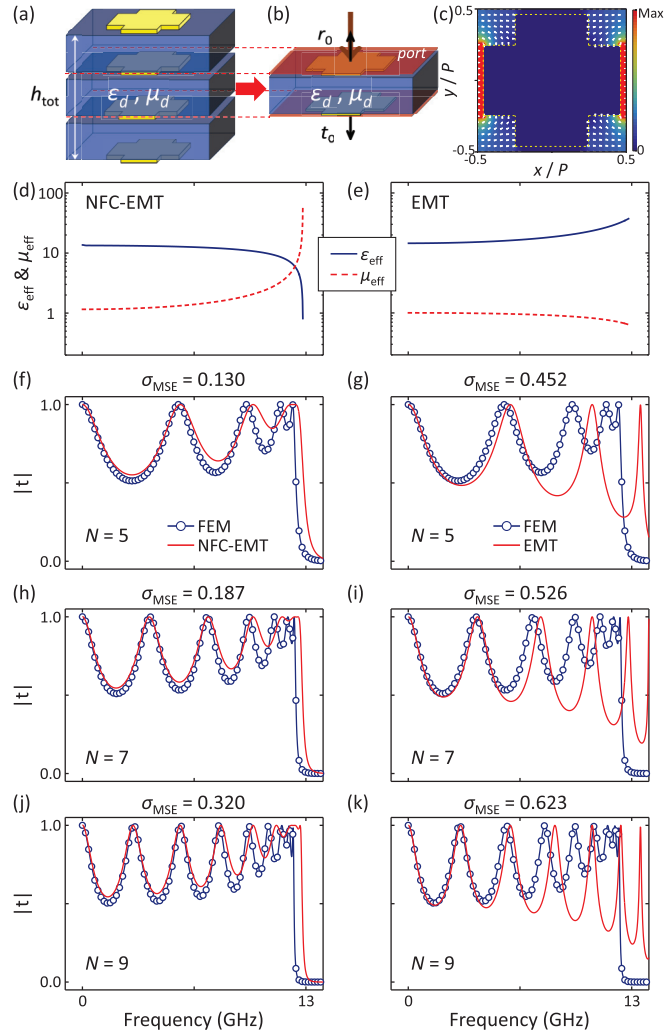

FIG. 6. (a),(b) Schematics of retrieving the effective parameters of an arbitrary multilayer metamaterial in the near-field-corrected effective-medium theory. Here, $\varepsilon_d = 3.5$, $\mu_d = 1$, and the metallic layer contains a periodic array (with lattice constant 6.5 mm) of metallic cross with geometric parameters: bar length 6 mm, bar width 3.2 mm, thickness 0.018 mm. The spacer thickness is 1.6 mm. (c) Finite-element-method-calculated *E*-field distributions (with color/arrow representing the amplitude/direction of the field and the yellow dashed line representing the profile of the microstructure) of the fundamental modes inside metallic regions. (d),(e) Frequency-dependent effective parameters calculated by (d) the near-field-corrected effective-medium theory and (e) the conventional effective-medium theory, respectively. (f),(h),(j) Transmission spectra computed by finite-element-method simulations (open circles) and the near-field-corrected effective-medium theory (solid lines) for metamaterials with $N = 5, 7, 9$. (g),(i),(k) Transmission spectra computed by finite-element-method simulations (open circles) and the conventional effective-medium theory (solid lines) for metamaterials with $N = 5, 7, 9$.

Repeating the same derivations as those in last section, we find that the effective parameters of such a metamaterial under

normally incident light with polarization σ_{inc} are given by two formulas very similar to Eq. (5):

$$\varepsilon_{\text{eff}} = \frac{2}{k_0 h_d \left|S^{\sigma_{\text{inc}}}_{\{0,0\},0}\right|^2}\sqrt{\alpha-\gamma}\sqrt{\alpha+\gamma}\left[\tan^{-1}\left(i\frac{\sqrt{\alpha-\gamma}}{\sqrt{\alpha+\gamma}}\right)+g\pi\right]$$

$$\mu_{\text{eff}} = \frac{2}{k_0 h_d}\frac{\left|S^{\sigma_{\text{inc}}}_{\{0,0\},0}\right|^2}{\sqrt{\alpha-\gamma}\sqrt{\alpha+\gamma}}\left[\tan^{-1}\left(i\frac{\sqrt{\alpha-\gamma}}{\sqrt{\alpha+\gamma}}\right)+g\pi\right], \tag{6}$$

where

$$\alpha = i\sum_{\{m_x,m_y\},\sigma}\left|S^{\sigma}_{\{m_x,m_y\},0}\right|^2 Y^{\text{III},\sigma}_{\{m_x,m_y\}}/Y^{\text{II}}_0\cot\left(k^{\text{III}}_{\{m_x,m_y\},z}h_d\right),$$

$$\gamma = i\sum_{\{m_x,m_y\},\sigma}\left|S^{\sigma}_{\{m_x,m_y\},0}\right|^2 Y^{\text{III},\sigma}_{\{m_x,m_y\}}/Y^{\text{II}}_0\csc\left(k^{\text{III}}_{\{m_x,m_y\},z}h_d\right),$$

$$S^{\sigma}_{\{m_x,m_y\},q} = \left(S^{\sigma}_{q,\{m_x,m_y\}}\right)^* = \frac{\int_{u.c.}\left(\vec{E}^{\sigma,\text{PW}}_{\{m_x,m_y\},||}\right)^*\cdot\vec{E}^{\text{Floquet}}_{q,||}dxdy}{\sqrt{\int_{u.c.}\left|\vec{E}^{\sigma,\text{PW}}_{\{m_x,m_y\},||}\right|^2 dxdy}\sqrt{\int_{u.c.}\left|\vec{E}^{\text{Floquet}}_{q,||}\right|^2 dxdy}} \tag{7}$$

with $\vec{E}^{\sigma,\text{PW}}_{\{m_x,m_y\},||}$ and $Y^{\text{III},\sigma}_{\{m_x,m_y\}}$ representing the parallel component of electric field and admittance of the diffraction mode with index $\{m_x, m_y\}$ and σ in the spacer region and Y^{II}_0 referring to the admittance of the fundamental quasi-transverse-electromagnetic mode in the metallic regime. Here, we follow the same strategy as described in the last section and again find it reasonable to choose the $g = 0$ branch of solutions for the one-layer subsystem. Obtaining the fundamental eigenmode of the complex metallic structure $\vec{E}^{\text{Floquet}}_{q=0}$ by full wave simulations [see Fig. 6(c)], we can then use Eqs. (6) and (7) to calculate the effective parameters of the system under study.

Figures 6(d) and 6(e) depict the frequency-dependent effective permittivity and permeability of the system, calculated by the near-field-corrected theory and conventional effective-medium theory, respectively. Similar to the system studied in the last section, here the effective parameters obtained with two different methods also exhibit opposite frequency dependencies. In particular, while μ_{eff} calculated by the near-field-corrected theory diverges at a specific frequency indicating the existence of a magnetic resonance, the same thing is not true for μ_{eff} obtained by the conventional effective-medium theory. We compare in Figs. 6(f)–6(k) the transmission spectra of three samples with different number of layers (N), calculated by two different versions of effective-medium theory with those calculated by the finite-element method on realistic structures. Obviously, our near-field-corrected theory performs much better than the conventional effective-medium theory, demonstrated by the much smaller values of σ_{MSE} for all cases studied.

We now experimentally validate our near-field-corrected effective-medium theory. We fabricate a five-layer metamaterial based on the design [Fig. 6(a)] with its top- and side-view pictures shown in Figs. 7(a) and 7(b), and then measure its transmission spectra in the microwave regime. Here, the interlayer spacers are made of F4BM350 (with $\varepsilon_r = 3.5$ and loss tangent 0.004). In our experiments, we illuminated the sample by normally incident y-polarized microwaves emitted from a horn antenna placed 1 m away from the sample, and then used another horn antenna placed 1 m away from the sample to collect the transmitted signals. Both the source and receiver antennas were connected to a vector-field analyzer (Agilent E8362c). Open circles in Figs. 7(c) and 7(d) depict the measured transmission spectrum for the five-layer metamaterial, which is in excellent agreement with the finite-element-method simulations. Most importantly, we find that the spectrum predicted by the near-field-corrected theory is obviously in much better agreement with our experimental results than the conventional effective-medium theory, in terms

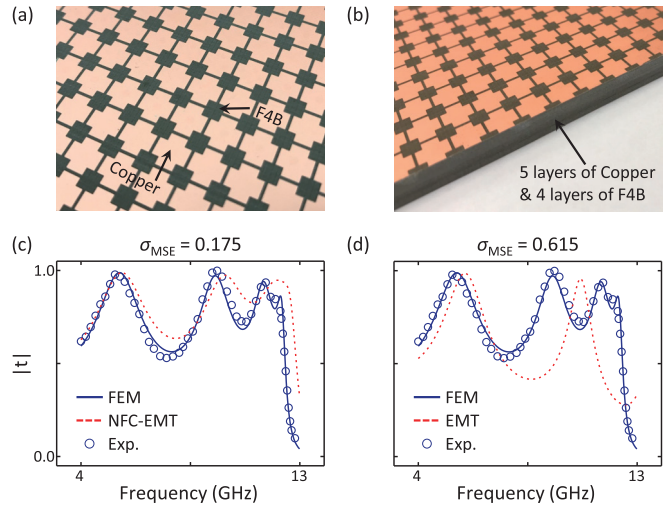

FIG. 7. (a) Top-view and (b) side-view pictures of the fabricated five-layer sample. Here, a metallic layer contains an array (with periodicity 6.5 mm) of metallic crosses with geometric parameters: bar length 6 mm, bar width 3.2 mm, and thickness 0.018 mm. The spacer thickness is 1.6 mm. (c) Spectra of transmission amplitude of the five-layer metamaterial, obtained by finite-element-method simulations (blue solid line), the near-field-corrected effective-medium theory (red dashed line), and experimental measurements (open circles). (d) Spectra of transmission amplitude of the five-layer metamaterial, obtained by finite-element-method simulations (blue solid line), the conventional effective-medium theory (red dashed line), and experimental measurements (open circles).

of both transmission-amplitude fluctuations (dictated by the effective impedance of the metamaterial) and the frequency positions of the transmission peaks (dictated by the effective refraction index of the metamaterial).

Before concluding this section, we discuss more about the applicable range of our effective-medium theory. First of all, we note that the near-field-corrected effective-medium theory does not apply to those systems with three-dimensional nonplanar microstructures, which *cannot* be "cut" from a plane inside the metallic layer. In addition, since our approach crucially relies on the assumption that excitations of high-order modes inside the metallic layers are weak enough to be dropped, we understand that the near-field-corrected theory will also break down when such an assumption is invalid. Since analytical solutions are difficult to obtain for microstructures with arbitrary shapes, we employ numerical approaches to explore when such single-mode approximation becomes invalid, still based on the metallic cross-shaped resonators. Here, we use $\chi = |S_{\{0,0\},0}|^2 / \sum_q |S_{\{0,0\},q}|^2$ as an indicator to tell whether the fundamental mode inside the metallic layer dominates the scattering process. We studied three different nine-layer metamaterials similar to those studied in Fig. 6(a), but with metallic "crosses" exhibiting different shapes [see Figs. 8(a)–8(c)]. For each shape, we continuously change the thickness of the spacer. As shown in Fig. 8, numerical calculations demonstrate that shrinking the size of the metallic "cross" decreases the values of χ, which suppresses the relative importance of the fundamental mode inside the metallic layer. As a result, the near-field-corrected effective-medium theory becomes less accurate as the size of metallic resonator decreases, reinforced by the increment of σ_{MSE} for the near-field-corrected theory. In other words, the near-field-corrected theory works better for systems with a higher ratio of metal occupations. In comparison, for systems with a lower ratio of metallic occupations, the conventional effective-medium theory is more applicable. Although such a trend is obtained through numerical simulations based on a specific microstructure, we expect it to be generally valid, which provides important guidance for the researchers to use our theory. Finally, we note that our near-field-corrected theory does not work well at high frequencies where electromagnetic fields can significantly penetrate inside the metallic layers, since strong near fields localized inside and outside plasmonic particles make it no longer reasonable to truncate the metallic layers as artificial boundaries.

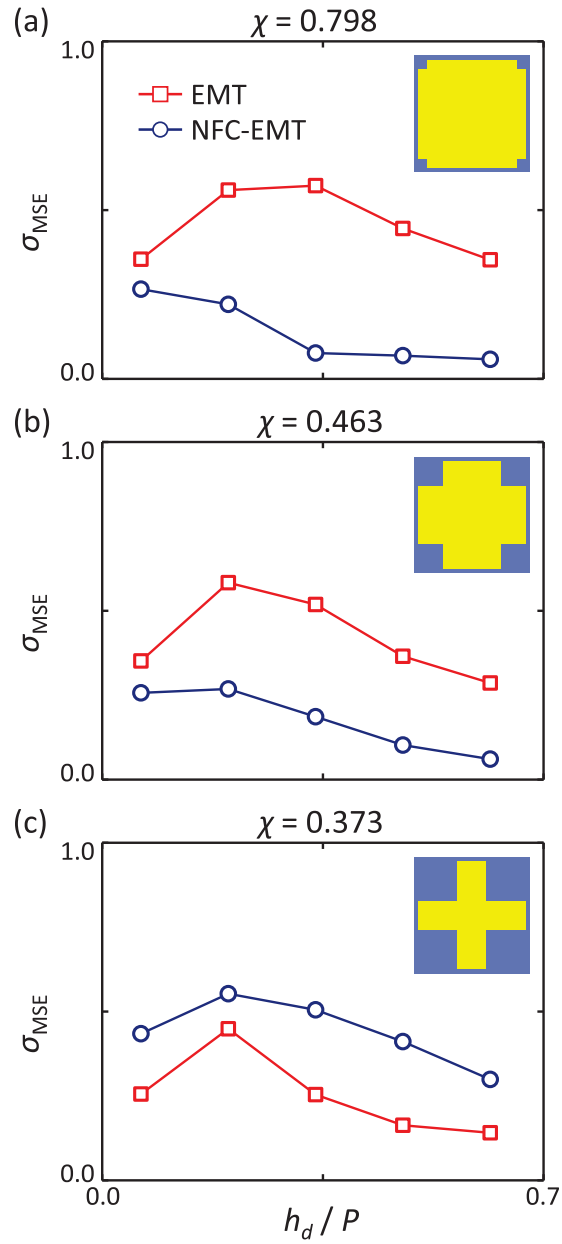

FIG. 8. σ_{MSE} and χ calculated with the near-field-corrected effective-medium theory (blue circles) and the effective-medium theory (red squares) on multilayer metamaterials consisting of cross-shaped metallic microstructures with varying spacer thickness h_d. Insets schematically depict the shapes of metallic resonators, with bar width being (a) 5.0 mm, (b) 3.2 mm, (c) 1.6 mm, respectively.

VI. CONCLUSION

To summarize, we propose an effective-medium theory to study strongly coupled multilayer metamaterials at low frequencies, in which the strong near-field couplings between adjacent metallic layers are automatically considered. The key idea is to choose a subsystem via cutting the realistic systems at the central planes of the metallic layers instead of the spacer layers. Comparisons with the conventional effective-medium theory show that our theory is particularly advantageous for studying those metamaterials with small interlayer distances, large total sizes, and a large area occupation ratio of metallic resonators at low frequencies, where the near-field couplings inside the spacer layers are very important while the high-order modes inside the metallic layers are less important. Our version of effective-medium theory well compliments the conventional effective-medium theory and is particularly useful for studying the strongly coupled metamaterials which have important applications in practice, justified by both numerical simulations and microwave experiments on realistic structures.

ACKNOWLEDGMENTS

This work was financially supported by National Natural Science Foundation of China (Grants No. 11734007,

No. 11674068, No. 91850101, and No. 11704240, Funder ID: http://dx.doi.org/10.13039/501100001809), National Key Research and Development Program of China (Grants No. 2017YFA0303504 and No. 2017YFA0700201), Shanghai Science and Technology Committee (Grants No. 20JC1414601, No. 20JC1414602, No. 17ZR1409500, and No. 18QA1401800), Shanghai East Scholar Plan, Fudan University-CIOMP Joint Fund (No. FC2018-006), FDUROP (Fudan's Undergraduate Research Opportunities Program) (No. 15079), and National University Student Innovation Program (No. 201510246068).

APPENDIX A: DERIVATION OF MODE-EXPANSION METHOD ON THE MODEL SYSTEM IN SEC. III

In region I, we expand the total electric field as

$$\vec{E}^{\mathrm{I}} = \vec{E}_0^{\mathrm{I,PW},-} + \sum_n \rho_n \vec{E}_n^{\mathrm{I,PW},+}, \tag{A1}$$

where $\vec{E}_0^{\mathrm{I,PW},-}$ represents the x-polarized normally incident plane wave (PW) and $\vec{E}_n^{\mathrm{I,PW},+}$ denotes the reflected plane wave propagating in the n th diffraction channel (with $k_{n,x}^{\mathrm{I}} = nG$ where $G = 2\pi/P$ and $n = 0, \pm 1, ...$) and ρ_n is the corresponding reflection coefficient. The parallel electric component takes the form $\vec{E}_{n,||}^{\mathrm{I,PW},\pm} = 1/\sqrt{P}\exp(ik_{n,x}^{\mathrm{I}}x)\exp[\pm ik_{n,z}^{\mathrm{I}}(z-h_m)]\hat{x}$. Meanwhile, in region II, the electric field can be expanded as linear combinations of a series of waveguide modes inside the slits. Specifically, the electric field inside the slit centered at x_j can be expanded as

$$\vec{E}^{\mathrm{II}} = \sum_q \left(a_q^+ \vec{E}_q^{\mathrm{II,WG},+} + a_q^- \vec{E}_q^{\mathrm{II,WG},-}\right), \quad |x - x_j| < a/2, \tag{A2}$$

where $\vec{E}_q^{\mathrm{II,WG},\pm}$ is the q th waveguide mode propagating along the $\pm z$ directions with $a_q^\pm$ denoting the corresponding expansion coefficients. The parallel electric field of the q th waveguide mode is $\vec{E}_{q,||}^{\mathrm{II,WG},\pm} = 1/\sqrt{2a(1+\delta_{q,0})}[\exp(ik_{q,x}^{\mathrm{II}}x) + (-1)^q\exp(-ik_{q,x}^{\mathrm{II}}x)]\exp(\pm ik_{q,z}^{\mathrm{II}}z)\hat{x}$ (with $k_{q,x}^{\mathrm{II}} = q\pi/a$ and $q = 0, 1, 2...$). We now consider electromagnetic eigenmodes in region III, which can be written as

$$\vec{E}^{\mathrm{III}} = \sum_m \left(b_m^+ \vec{E}_m^{\mathrm{III,SC},+} + b_m^- \vec{E}_m^{\mathrm{III,SC},-}\right), \tag{A3}$$

where $b_m^\pm$ are the coefficients for the m th scattering mode with normalized wave functions, $\vec{E}_{m,||}^{\mathrm{III,SC},\pm} = 1/\sqrt{P}\exp(ik_{m,x}^{\mathrm{III}}x)\exp(\pm ik_{m,z}^{\mathrm{III}}z)\hat{x}$ (with $k_{m,x}^{\mathrm{III}} = mG$ and $m = 0, \pm 1, ...$). Electromagnetic waves inside regions IV and VI can be studied in a similar way to region II, where the total electric fields inside the slit centered at x_j can be expanded as

$$\vec{E}^{\mathrm{IV}} = \sum_q \left(c_q^+ \vec{E}_q^{\mathrm{IV,WG},+} + c_q^- \vec{E}_q^{\mathrm{IV,WG},-}\right), \quad |x - x_j| < a/2$$

$$\vec{E}^{\mathrm{VI}} = \sum_q \left(e_q^+ \vec{E}_q^{\mathrm{VI,WG},+} + e_q^- \vec{E}_q^{\mathrm{VI,WG},-}\right), \quad |x - x_j| < a/2, \tag{A4}$$

where $c_q^\pm$ and $e_q^\pm$ are the mode coefficients for the qth waveguide mode in these two regions. Given the position of the $z = 0$ plane, the parallel electric components of the q th waveguide mode in regions IV and VI are slightly different from those in region II. They are $\vec{E}_{q,||}^{\mathrm{IV,WG},\pm} = 1/\sqrt{2a(1+\delta_{q,0})}[\exp(ik_{q,x}^{\mathrm{IV}}x) + (-1)^q\exp(-ik_{q,x}^{\mathrm{IV}}x)]\exp[\pm ik_{q,z}^{\mathrm{IV}}(z+h_d)]\hat{x}$ and $\vec{E}_{q,||}^{\mathrm{VI,WG},\pm} = 1/\sqrt{2a(1+\delta_{q,0})}[\exp(ik_{q,x}^{\mathrm{VI}}x) + (-1)^q\exp(-ik_{q,x}^{\mathrm{VI}}x)]\exp[\pm ik_{q,z}^{\mathrm{VI}}(z+2h_d+h_m)]\hat{x}$ respectively (with $k_{q,x}^{\mathrm{IV}} = k_{q,x}^{\mathrm{VI}} = k_{q,x}^{\mathrm{II}}$). In region V, the electric field can be studied in a similar way to region III, with the total electric fields

$$\vec{E}^{\mathrm{V}} = \sum_m \left(d_m^+ \vec{E}_m^{\mathrm{V,SC},+} + d_m^- \vec{E}_m^{\mathrm{V,SC},-}\right), \tag{A5}$$

where $d_m^\pm$ are the corresponding coefficients and $\vec{E}_{m,||}^{\mathrm{V,SC},\pm} = 1/\sqrt{P}\exp(ik_{m,x}^{\mathrm{V}}x)\exp[\pm ik_{m,z}^{\mathrm{V}}(z+h_d+h_m)]\hat{x}$ (with $k_{m,x}^{\mathrm{V}} = k_{m,x}^{\mathrm{III}}$). Finally, the electric field in region VII is

$$\vec{E}^{\mathrm{VII}} = \sum_n t_n \vec{E}_n^{\mathrm{VII,PW},-}, \tag{A6}$$

where t_n are the expansion coefficients and $\vec{E}_{n,||}^{\mathrm{VII,PW},-} = 1/\sqrt{P}\exp(ik_{n,x}^{\mathrm{VII}}x)\exp[-ik_{n,z}^{\mathrm{VII}}(z+2h_m+2h_d)]\hat{x}$ (with $k_{n,x}^{\mathrm{VII}} = k_{n,x}^{\mathrm{I}}$). In all these regions, magnetic fields can be derived from the electric fields using Maxwell's equations. We also note that the perpendicular wave vectors are determined by the dispersion relation $(k_{n,x}^{\mathrm{i}})^2 + (k_{n,z}^{\mathrm{i}})^2 = \varepsilon_{\mathrm{i}}(\omega/c)^2$, where ω and c denote the frequency and speed of light in the i th region (i = I, II, III, IV, V, VI, VII), and $\varepsilon_{\mathrm{I}} = \varepsilon_{\mathrm{II}} = \varepsilon_{\mathrm{IV}} = \varepsilon_{\mathrm{VI}} = \varepsilon_{\mathrm{VII}} = 1$, $\varepsilon_{\mathrm{III}} = \varepsilon_{\mathrm{V}} = \varepsilon_d$ are the permittivity in each region.

By matching the boundary condition for electric field at the $z = h_m$ interface and using the orthonormal conditions $\int_{-P/2}^{P/2}(\vec{E}_{n,||}^{\mathrm{PW}})^* \cdot \vec{E}_{n',||}^{\mathrm{PW}}dx = \delta_{n,n'}$, we obtain that

$$\rho_n + \delta_{n,0} = \sum_q S_{nq}^{(1,2)}\left[a_q^+ \exp\left(ik_{q,z}^{\mathrm{II}}h_m\right) + a_q^- \exp\left(-ik_{q,z}^{\mathrm{II}}h_m\right)\right], \tag{A7}$$

where the coupling strength is

$$\begin{aligned} S_{nq}^{(1,2)} &= \int_{-P/2}^{P/2}\left(\vec{E}_{n,||}^{\mathrm{I,PW}}\right)^* \cdot \vec{E}_{q,||}^{\mathrm{II,WG}}dx \\ &= \sqrt{\frac{a}{2P\cdot(1+\delta_{q,0})}}[\mathrm{sinc}(n\pi\cdot a/P - q\pi/2) \\ &\quad + (-1)^q\cdot\mathrm{sinc}(n\pi\cdot a/P + q\pi/2)]. \end{aligned} \tag{A8}$$

Similarly, matching the boundary condition for magnetic field at this interface and using the orthonormal conditions $\int_{-a/2}^{a/2}(\vec{E}_{q,||}^{\mathrm{II,WG}})^* \cdot \vec{E}_{q',||}^{\mathrm{II,WG}}dx = \delta_{q,q'}$, we have

$$\begin{aligned} \sum_n S_{qn}^{(2,1)}Y_n^{\mathrm{I}}[\rho_n - \delta_{n,0}] = Y_q^{\mathrm{II}}\big[&a_q^+\exp\left(ik_{q,z}^{\mathrm{II}}h_m\right) \\ &- a_q^-\exp\left(-ik_{q,z}^{\mathrm{II}}h_m\right)\big], \end{aligned} \tag{A9}$$

where the overlapping integrals are $S_{qn}^{(2,1)} = \int_{-P/2}^{P/2}(\vec{E}_{q,||}^{\mathrm{II,WG}})^* \cdot \vec{E}_{n,||}^{\mathrm{I,PW}}dx = (S_{nq}^{(1,2)})^*$.

Matching the tangential components of electric and magnetic fields at other interfaces between adjacent regions and employing the orthonormal conditions of these eigenmodes, we get the following set of coupled linear equations:

$$\begin{aligned}
\rho_n + \delta_{n,0} &= \sum_q S_{nq}^{(1,2)}\left[a_q^+ \exp\left(ik_{q,z}^{\mathrm{II}} h_m\right) + a_q^- \exp\left(-ik_{q,z}^{\mathrm{II}} h_m\right)\right] \\
\sum_n S_{qn}^{(2,1)} Y_n^{\mathrm{I}}(\rho_n - \delta_{n,0}) &= Y_q^{\mathrm{II}}\left[a_q^+ \exp\left(ik_{q,z}^{\mathrm{II}} h_m\right) - a_q^- \exp\left(-ik_{q,z}^{\mathrm{II}} h_m\right)\right] \\
b_m^+ + b_m^- &= \sum_q S_{mq}^{(3,2)}(a_q^+ + a_q^-) \\
\sum_m S_{qm}^{(2,3)} Y_m^{\mathrm{III}}(b_m^+ - b_m^-) &= Y_q^{\mathrm{II}}(a_q^+ - a_q^-) \\
b_m^+ \exp\left(-ik_{m,z}^{\mathrm{III}} h_d\right) + b_m^- \exp\left(ik_{m,z}^{\mathrm{III}} h_d\right) &= \sum_q S_{mq}^{(3,4)}(c_q^+ + c_q^-) \\
\sum_m S_{qm}^{(4,3)} Y_m^{\mathrm{III}}\left[b_m^+ \exp\left(-ik_{m,z}^{\mathrm{III}} h_d\right) - b_m^- \exp\left(ik_{m,z}^{\mathrm{III}} h_d\right)\right] &= Y_q^{\mathrm{IV}}(c_q^+ - c_q^-) \\
d_m^+ + d_m^- &= \sum_q S_{mq}^{(5,4)}\left[c_q^+ \exp\left(-ik_{q,z}^{\mathrm{IV}} h_m\right) + c_q^- \exp\left(ik_{q,z}^{\mathrm{IV}} h_m\right)\right] \\
\sum_m S_{qm}^{(4,5)} Y_m^{\mathrm{V}}(d_m^+ - d_m^-) &= Y_q^{\mathrm{IV}}\left[c_q^+ \exp\left(-ik_{q,z}^{\mathrm{IV}} h_m\right) - c_q^- \exp\left(ik_{q,z}^{\mathrm{IV}} h_m\right)\right] \\
d_m^+ \exp(-ik_{m,z}^{\mathrm{V}} h_d) + d_m^- \exp(ik_{m,z}^{\mathrm{V}} h_d) &= \sum_q S_{mq}^{(5,6)}(e_q^+ + e_q^-) \\
\sum_m S_{qm}^{(6,5)} Y_m^{\mathrm{V}}\left[d_m^+ \exp\left(-ik_{m,z}^{\mathrm{V}} h_d\right) - d_m^- \exp\left(ik_{m,z}^{\mathrm{V}} h_d\right)\right] &= Y_q^{\mathrm{VI}}(e_q^+ - e_q^-) \\
t_n^- &= \sum_q S_{nq}^{(7,6)}\left[e_q^+ \exp\left(-ik_{q,z}^{\mathrm{VI}} h_m\right) + e_q^- \exp\left(ik_{q,z}^{\mathrm{VI}} h_m\right)\right] \\
-\sum_n S_{qn}^{(6,7)} Y_n^{\mathrm{VII}} t_n^- &= Y_q^{\mathrm{VI}}\left[e_q^+ \exp\left(-ik_{q,z}^{\mathrm{VI}} h_m\right) - e_q^- \exp\left(ik_{q,z}^{\mathrm{VI}} h_m\right)\right]. \qquad \text{(A10)}
\end{aligned}$$

Here, $Y_n^{\mathrm{i}} = \omega\varepsilon_{\mathrm{i}}/k_{n,z}^{\mathrm{i}}$ denotes the admittance for the n th mode in the i th region, $S_{nq}^{(\mathrm{i,j})} = \int_{-a/2}^{a/2} (\vec{E}_n^{\mathrm{i,PW}})^* \cdot \vec{E}_q^{\mathrm{j,WG}} dx = (S_{qn}^{(\mathrm{j,i})})^*$ denotes the overlapping integral between the n th diffracting plane wave in i th region and the q th waveguide mode inside the slit in j th region, and $S_{mq}^{(\mathrm{k,j})} = \int_{-a/2}^{a/2} (\vec{E}_m^{\mathrm{k,SC}})^* \cdot \vec{E}_q^{\mathrm{j,WG}} dx = (S_{qm}^{(\mathrm{j,k})})^*$ has a similar definition. Solving Eq. (A10), we thus obtain all scattering coefficients.

APPENDIX B: DERIVATION OF EQ. (2)

Consider the wave scattering problem as depicted in Fig. 4(b). We assume that the incident wave coming from the semi-infinite grating medium is the fundamental waveguide mode inside the grating taking a unit amplitude, and then calculate the transmitted and reflected waves inside the semi-infinite media below and above the system. The transmitted/reflected waves can be expressed to linear combinations of different waveguide modes with appropriate coefficients, which can be obtained by solving the following coupled equations:

$$\begin{aligned}
b_m^+ + b_m^- &= \sum_q S_{mq}^{(3,2)} \rho_q^{\mathrm{single}} \exp\left(-ik_{q,z}^{\mathrm{II}} \frac{h_m}{2}\right) + S_{m0}^{(3,2)} \exp\left(ik_{q,z}^{\mathrm{II}} \frac{h_m}{2}\right) \\
\sum_m S_{qm}^{(2,3)} Y_m^{\mathrm{III}}(b_m^+ - b_m^-) &= Y_q^{\mathrm{II}} \rho_q^{\mathrm{single}} \exp\left(-ik_{q,z}^{\mathrm{II}} \frac{h_m}{2}\right) - Y_0^{\mathrm{II}} \exp\left(ik_{q,z}^{\mathrm{II}} \frac{h_m}{2}\right) \\
b_m^+ \exp\left(-ik_{m,z}^{\mathrm{III}} h_d\right) + b_m^- \exp\left(ik_{m,z}^{\mathrm{III}} h_d\right) &= \sum_q S_{mq}^{(3,4)} t_q^{\mathrm{single}} \exp\left(-ik_{q,z}^{\mathrm{II}} \frac{h_m}{2}\right) \\
\sum_m S_{qm}^{(4,3)} Y_m^{\mathrm{III}}\left[b_m^+ \exp\left(-ik_{m,z}^{\mathrm{III}} h_d\right) - b_m^- \exp\left(ik_{m,z}^{\mathrm{III}} h_d\right)\right] &= -Y_q^{\mathrm{IV}} t_q^{\mathrm{single}} \exp\left(-ik_{q,z}^{\mathrm{II}} \frac{h_m}{2}\right). \qquad \text{(B1)}
\end{aligned}$$

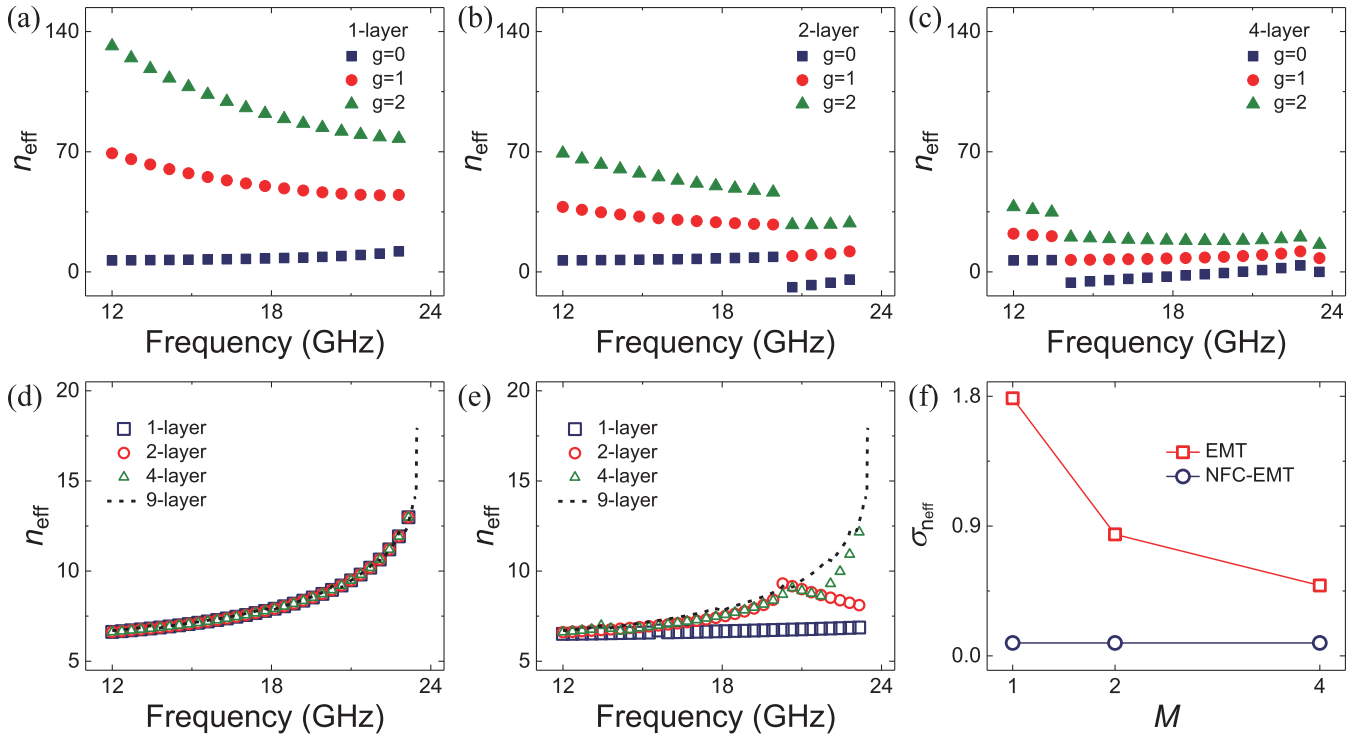

FIG. 9. Effective-medium parameters calculated by NFC-EMT for subsystems with (a) one layer, (b) two layers, and (c) four layers with different branches. Effective-medium parameters calculated by (d) NFC-EMT and (e) conventional EMT for structures with different layers with proper branches selected. (f) $\sigma_{n_{\text{eff}}}$ calculated with NFC-EMT (blue circles) and conventional EMT (red squares) for a nine-layer structure vs number of layers (M) taken into account for homogenization.

Assuming $h_m = 0$ since $h_m/\lambda \to 0$ (valid at low frequencies) and using the thin-slit approximation to drop all high order expansion coefficients ($|S_{m0}|^2 \gg |S_{mq}|^2$, $q \neq 0$), we get from Eq. (B1) the following set of equations:

$$\begin{aligned} b_m^+ + b_m^- &= S_{m0}^{(3,2)}\left(\rho_0^{\text{single}} + 1\right) \\ \sum_m S_{0m}^{(2,3)} Y_m^{\text{III}}\left(b_m^+ - b_m^-\right) &= Y_0^{\text{II}}\left(\rho_0^{\text{single}} - 1\right) \\ b_m^+ \exp\left(-ik_{m,z}^{\text{III}} h_d\right) + b_m^- \exp\left(ik_{m,z}^{\text{III}} h_d\right) &= S_{m0}^{(3,4)} t_0^{\text{single}} \\ \sum_m S_{0m}^{(4,3)} Y_m^{\text{III}}\left[b_m^+ \exp\left(-ik_{m,z}^{\text{III}} h_d\right) - b_m^- \exp\left(ik_{m,z}^{\text{III}} h_d\right)\right] &= -Y_0^{\text{IV}} t_0^{\text{single}} \end{aligned} \tag{B2}$$

to determine the specular reflection and transmission coefficients. Solving Eq. (B2), we get the explicit expressions for ρ_0^{single} and t_0^{single}, which are just Eq. (2) in the main text.

APPENDIX C: DISCUSSIONS ON BRANCH-SELECTION ISSUES OF EQS. (4) AND (5)

We use the nine-layer metamaterial described in Sec. IV as a specific example to illustrate how to choose the correct branch in our theory. Figures 9(a)–9(c) depict, respectively, the frequency-dependent effective refractive indices n_{eff} of the metamaterial, calculated with our theory based on subsystems containing one, two, and four layers of our periodic structure. Obviously, in all cases studied, we always get multiple branches of n_{eff} solutions specified by the value of g. At every frequency, we choose the correct solution of n_{eff} based on the criterion that calculations based on different subsystems should yield identical (at least nearly identical) values. Based on such a criterion, we find that the first branch in one-layer calculations is the correct one, as n_{eff} thus obtained match very well with calculations with other subsystems (even including the nine-layer system) at all frequencies studied [see Fig. 9(d)]. Obviously, n_{eff} solutions on other branches in one-layer calculations do not merge well with their counterparts in two-layer and four-layer calculations. Therefore, we conclude that the results presented in Fig. 9(d) are the desired ones. In sharp contrast, as we repeated all the above calculations based on a conventional effective-medium theory, we found that results calculated based on different subsystems, even with proper branches selected in each case, do not match well with each other [Fig. 9(e)].

The excellent agreement among results obtained with different subsystems further reveal an important advantage of our theory, that is, a one-layer subsystem is sufficient to obtain the converged final results. This is physically sound, because the one-layer subsystem exhibits a deep-subwavelength thickness ($h_d \ll \lambda$) and thus the $g = 0$ branch naturally describes the fundamental mode propagating in such a subsystem. Quanti-

tatively, we computed the averaged deviations ($\sigma_{n_{\text{eff}}}$) between n_{eff} obtained with M-layer and nine-layer calculations within the frequency domain of interest (12.0–23.5 GHz), and show in Fig. 9(f) how $\sigma_{n_{\text{eff}}}$ varies against the number of layers (M). Circles in Fig. 9(f) indicate that the convergence of n_{eff} against the thickness of subsystem (M) is very fast in our theory. In sharp contrast, we repeated all calculations with the conventional EMT, and found that such convergence is much slower in conventional EMT, and one needs to use a thicker subsystem to obtain reliable results using the conventional EMT [see red squares in Fig. 9(f)].

APPENDIX D: NUMERICAL SIMULATIONS

All numerical simulation results in this paper were obtained by finite-element-method simulations using a numerical solver (COMSOL Multiphysics). In our simulations, we consider a unit cell of the simulated structure with periodic boundary conditions imposed. We measure the reflected and transmitted signals at two planes (ports) placed at two to three wavelengths away from the metamaterial to ensure that no near fields generated by the inhomogeneous structure can reach the ports.

[1] J. B. Pendry, A. J. Holden, W. J. Stewart, and I. Youngs, Phys. Rev. Lett. **76**, 4773 (1996).

[2] J. B. Pendry, A. J. Holden, D. J. Robbins, and W. J. Stewart, IEEE Trans. Microw. Theory Technol. **47**, 2075 (1999).

[3] D. R. Smith, W. J. Padilla, D. C. Vier, S. C. Nemat-Nasser, and S. Schultz, Phys. Rev. Lett. **84**, 4184 (2000).

[4] C. M. Soukoulis and M. Wegener, Nat. Photonics **5**, 523 (2011).

[5] R. A. Shelby, D. R. Smith, and S. Schultz, Science **292**, 77 (2001).

[6] J. B. Pendry, Phys. Rev. Lett. **85**, 3966 (2000).

[7] N. Fang, H. Lee, C. Sun, and X. Zhang, Science **308**, 534 (2005).

[8] N. I. Landy, S. Sajuyigbe, J. J. Mock, D. R. Smith, and W. J. Padilla, Phys. Rev. Lett. **100**, 207402 (2008).

[9] J. Hao, L. Zhou, and M. Qiu, Phys. Rev. B **83**, 165107 (2011).

[10] X. Shen, T. J. Cui, J. Zhao, H. F. Ma, W. X. Jiang, and H. Li, Opt. Express **19**, 9401 (2011).

[11] J. Hao, Y. Yuan, L. Ran, T. Jiang, J. A. Kong, C. T. Chan, and L. Zhou, Phys. Rev. Lett. **99**, 063908 (2007).

[12] S. Xiao, H. Mühlenbernd, G. Li, M. Kenney, F. Liu, T. Zentgraf, S. Zhang, and J. Li, Adv. Opt. Mater. **4**, 654 (2016).

[13] S. Xiao, J. Wang, F. Liu, S. Zhang, X. Yin, and J. Li, Nanophotonics **6**, 215 (2017).

[14] D. R. Smith, S. Schultz, P. Markoš, and C. M. Soukoulis, Phys. Rev. B **65**, 195104 (2002).

[15] T. Feng, F. Liu, W. Y. Tam, and J. Li, Europhys. Lett. **102**, 18003 (2013).

[16] D. R. Smith and J. B. Pendry, J. Opt. Soc. Am. B **23**, 391 (2006).

[17] J. Shin, J. T. Shen, and S. Fan, Phys. Rev. Lett. **102**, 093903 (2009).

[18] P. Sheng, *Introduction to Wave Scattering, Localization, and Mesoscopic Phenomena* (Academic Press, San Diego, 1995).

[19] T. Decoopman, G. Tayeb, S. Enoch, D. Maystre, and B. Gralak, Phys. Rev. Lett. **97**, 073905 (2006).

[20] Y. Wu, J. Li, Z. Q. Zhang, and C. T. Chan, Phys. Rev. B **74**, 085111 (2006).

[21] S. Sun, S. T. Chui, and L. Zhou, Phys. Rev. E **79**, 066604 (2009).

[22] F. Monticone, N. M. Estakhri, and A. Alu, Phys. Rev. Lett. **110**, 203903 (2013).

[23] C. Pfeiffer, N. K. Emani, A. M. Shaltout, A. Boltasseva, V. M. Shalaev, and A. Grbic, Nano Lett. **14**, 2491 (2014).

[24] H. Guo, J. Lin, M. Qiu, J. Tian, Q. Wang, Y. Li, S. Sun, Q. He, S. Xiao, and L. Zhou, J. Phys. D: Appl. Phys. **51**, 074001 (2018).

[25] B. Yang, T. Liu, H. Guo, S. Xiao, and L. Zhou, Sci. Bull. **64**, 823 (2019).

[26] J. Zhou, T. Koschny, M. Kafesaki, and C. M. Soukoulis, Photonics Nanostruct. Fundam. Appl. **6**, 96 (2008).

[27] C. Rockstuhl, T. Paul, F. Lederer, T. Pertsch, T. Zentgraf, T. P. Meyrath, and H. Giessen, Phys. Rev. B **77**, 035126 (2008).

[28] J. T. Shen, P. B. Catrysse, and S. Fan, Phys. Rev. Lett. **94**, 197401 (2005).

[29] M. Choi, S. H. Lee, Y. Kim, S. B. Kang, J. Shin, M. H. Kwak, K. Y. Kang, Y. H. Lee, N. Park, and B. Min, Nature (London) **470**, 369 (2011).

[30] X. Yang, J. Yao, J. Rho, X. Yin, and X. Zhang, Nat. Photonics **6**, 450 (2012).

[31] F. J. García-Vidal, L. Martín-Moreno, and J. B. Pendry, J. Opt. A: Pure Appl. Opt. **7**, S97 (2005).

[32] J. Bravo-Abad, F. J. García-Vidal, and L. Martín-Moreno, Phys. Rev. Lett. **93**, 227401 (2004).

[33] S. Xiao, Q. He, C. Qu, X. Li, S. Sun, and L. Zhou, Opt. Express **21**, 27219 (2013).

[34] S. Ma, S. Xiao, and L. Zhou, Phys. Rev. B **93**, 045305 (2016).

[35] S. Tang, B. Zhu, M. Jia, Q. He, S. Sun, Y. Mei, and L. Zhou, Phys. Rev. B **91**, 174201 (2015).